Elucidating the Gas-Phase Behavior of Nitazene Analog Protomers using Structures for Lossless Ion Manipulations Ion Mobility-Orbitrap Mass Spectrometry

Adam L. Hollerbach[1*], Vivian S. Lin[1], Yehia M. Ibrahim[1], Robert G. Ewing[2], Thomas O. Metz[1], Kabrena E. Rodda[2]

[1] Biological Sciences Division, Pacific Northwest National Laboratory, Richland, Washington, 99354, United States

[2] Nuclear, Chemistry & Biology Division, Pacific Northwest National Laboratory, Richland, Washington, 99354, United States

Corresponding Author

* adam.hollerbach@pnnl.gov

Abstract

2-benzylbenzimidazoles, or "nitazenes", are a class of novel synthetic opioids (NSOs) that are increasingly being detected alongside fentanyl analogs and other opioids in drug overdose cases. Nitazenes can be 20x more potent than fentanyl but are not routinely tested for during postmortem or clinical toxicology drug screens; thus, their prevalence in drug overdose cases may be under-reported. Traditional analytical workflows utilizing liquid chromatography-tandem mass spectrometry (LC-MS/MS) often require additional confirmation with authentic reference standards to identify a novel nitazene. However, additional analytical measurements with ion mobility spectrometry (IMS) may provide a path towards reference-free identification, which would greatly accelerate NSO identification rates in toxicology labs. Presented here are the first IMS and collision cross section (CCS) measurements on a set of fourteen nitazene analogs using a Structures for Lossless Ion Manipulations (SLIM)-Orbitrap MS. All nitazenes exhibited two high intensity baseline-separated IMS distributions, which fentanyls and other drug and drug-like compounds also exhibit. Incorporating water into the electrospray ionization (ESI) solution caused the intensities of the higher mobility IMS distributions to increase the intensities of the lower mobility IMS distributions to decrease. Nitazenes lacking a nitro group at the R1 position exhibited the greatest shifts in signal intensities due to water. Furthermore, IMS-MS/MS experiments showed that the higher mobility IMS distributions of all nitazenes produced fragment ions with *m/z* 72, 100, and other low intensity fragments while the lower mobility IMS distributions only produced fragment ions with *m/z* 72 and 100. The IMS, solvent, and fragmentation studies provide experimental evidence that nitazenes potentially exhibit three gas-phase protomers. The cyclic IMS capability of SLIM was also employed to partially resolve four sets of structurally similar nitazene isomers (e.g., protonitazene/isotonitazene, butonitazene/isobutonitazene/secbutonitazene), showcasing the potential of using high-resolution IMS separations in MS-based workflows for reference-free identification of emerging nitazenes and other NSOs.

Keywords: analog, CID, electrospray ionization, nitazene, gas-phase, high resolution, ion mobility, mass accuracy, mass spectrometry, NSO, opioid, Orbitrap, protomer, SLIM, traveling wave

Introduction

According to the Center for Disease Control (CDC), drug-related overdoses contributed to ~108,000 deaths in the United States in 2022.[1] Novel synthetic opioids (NSOs), including primarily fentanyl and fentanyl analogs, accounted for ~70% of these deaths, which is 22x higher than ten years ago.[1,2] NSOs other than fentanyl, along with other sedatives, have been detected throughout the United States with increasing frequency since 2017.[3] In particular, nitazenes, a class of NSOs known as the 2-benzylbenzimidazoles, are rapidly increasing their prevalence in fentanyl overdose cases.[4] Nitazenes were first synthesized by the pharmaceutical company CIBA Aktiengesellschaft in 1957, which was two years before the first synthesis of fentanyl by Paul Janssen.[5] But unlike fentanyl, nitazenes were never approved for clinical use in humans.[6] Nitazenes possess three structural features that distinguishes them from other NSOs: (1) a benzimidazole core, (2) a 2-benzyl ring, and (3) a 1-ethylamino group with two potential substitutions (see Figure S1 in the Supporting Information). Many nitazene analogs, such as etonitazene and isotonitazene, exhibit strong affinity for the mu opioid receptor and can exhibit up to ~20x higher potencies than fentanyl and many fentanyl analogs.[7] Vandeputte et al. also found that a metabolite of isotonitazene, N-desethylisotonitazene, exhibits a 2.6x greater potency than its parent compound, which could potentially increase the chances of overdose.[7] The Drug Enforcement Agency (DEA) has begun scheduling many nitazenes due to their high potential for abuse.[8] But as has happened with fentanyls, the scheduling of certain nitazenes has resulted in the development of new nitazene analogs that are either not scheduled, avoid detection using conventional technologies, or both.[3] There is thus a need to develop new technologies and methods that can detect and identify nitazenes in a general manner.

Many different technologies have been developed to detect NSOs and they can be loosely grouped into two categories: (1) relatively simple technologies like test strips,[9,10] and (2) advanced technologies that employ sophisticated analytical instrumentation like Raman spectroscopy,[8,11] mass spectrometry (MS) and/or tandem mass spectrometry (MS/MS),[12-18] and ion mobility spectrometry (IMS).[19-22] Test strips (colorimetric and immunoassay-based) are fast, cheap, and easy to use, but they are chemically specific. Test strips may also yield false positives when testing mixtures in which other compounds are present with NSOs[10] or false negatives as they may not detect all the possible analogs of a class of NSOs.[9]

Alternatively, the advanced technologies are nonspecific and can be used to analyze many different NSOs simultaneously. MS is one of the most widely used advanced techniques for detecting NSOs due to its low limits of detection, fast analysis speed, and readiness for coupling with orthogonal separation techniques like liquid chromatography (LC).[23,24] High-resolution MS (HR-MS) and MS/MS can be used to identify specific chemical signatures of NSOs that distinguish them from other compounds. For example, fentanyls are known to produce two high intensity ESI-based MS/MS fragments that correspond to cleavages at two different amine sites (e.g., *m/z* 105,188).[25] The *m/z* of these MS/MS peaks can differ if a fentanyl analog possesses a functional group added to the piperidine ring or to a moiety attached to the piperidinyl nitrogen, such as an ethylbenzene ring. When this information is combined with the presence of other lower intensity fragment ions, it can help determine if an unknown ion is a fentanyl analog, and sometimes even its chemical structure. Most nitazenes also produce two primary ESI-based fragments with *m/z* 100 and 72, which corresponds to triethylamine and N,N-diethylamine fragment ions, respectively.[7,26] There are often other lower intensity fragment ions that can be used to distinguish between nitazene analogs.[27] However, most nitazenes exhibit the same two primary fragment ions (*m/z* 72, *m/z* 100), meaning that MS/MS spectra alone may not provide enough information to differentiate nitazene isomers from each other, or possibly from other coexisting isobaric ions (ions with the same *m/z* but different chemical structures).

Researchers have addressed the issue of differentiating nitazene isomers by coupling LC to MS, and at least three independent groups have shown that LC can readily separate the positional isomers protonitazene (propyl group) and isotonitazene (isopropyl group), as well as other nitazene isomers.[3,26,27] Kanamori et al. also demonstrated that gas chromatography (GC) can separate isoprotonitazene (propyl group) and iso-isotonitazene (isopropyl group), which are also positional isomers.[27] To date there have been no published studies that used ion mobility spectrometry (IMS) to analyze nitazenes. IMS is an analytical technique known for its ability to distinguish between structural isomers and is increasingly being incorporated into routine MS-based screening methods for analyzing NSOs.[28] IMS separates gas-phase ions based on their size, shape, charge, and interaction with a buffer gas in the presence of an electric field.[29,30] A rotationally averaged ion-neutral collision cross section (CCS) can be measured with IMS, and this measurement, along with theoretical modeling, can provide information about ion gas-phase structure.[31,32] Many commercial IMS systems employ drift tubes (DT), which provide low resolution IMS separations

with resolving powers typically ~50.[20,33] More recently high-resolution IMS systems such as cyclic IMS and trapped ion mobility spectrometry (TIMS) have become commercially available and can provide resolving powers of over 200.[34-36] However, high IMS resolving powers are needed to separate NSOs with high structural similarity, such as structural isomers of nitazenes (e.g., protonitazene and isotonitazene). IMS resolving powers have recently been greatly improved through the development of high-resolution IMS systems like traveling wave-based structures for lossless ion manipulations (SLIM), which have provided IMS resolving powers of over 1000 and have allowed compounds with very small structural differences (e.g., less than 0.01 $Å^2$ difference) to be separated with IMS.[37-40]

Both low-resolution and high-resolution IMS have recently been used to show that specific NSOs, like fentanyl, exhibit diagnostic gas-phase behavior that can be used to aid in their detection. In 2019, Zaknoun and coworkers were working with an atmospheric pressure DT-IMS and a radioactive nickel source and discovered that fentanyl and fentanyl analogs exhibit multiple IMS distributions instead of just one,[19] whereas other opioids like heroin, morphine, codeine, hydrocodone, and methadone only exhibit single IMS distributions.[20,41] Butler and Baker proposed that the two IMS distributions of fentanyl they observed using electrospray ionization and a low pressure drift tube were either gas-phase conformers (e.g., rotomers) or protomers (i.e., gas-phase conformations adopted due to differences in the protonation site).[20] Hollerbach et al. later performed a comprehensive set of experiments demonstrating that the intensities of the two IMS distributions of all fentanyls change as a function of water concentration in the electrospray solvent,[22] which is known behavior of other compounds that exhibit protomers (e.g., para-aminobenzoic acid).[42] Additionally, both Hollerbach et al. and Aderorho et al. found that the two IMS distributions produce different fragmentation spectra, which is also expected behavior of protomers.[22,43] It is worth noting that the reduced mobility values obtained with atmospheric pressure IMS systems are sensitive to impurities in the buffer gas (e.g., water) and clustering effects (e.g., from mixtures of analytes).[44,45] Large mobility shifts can occur if both are not properly controlled, and this can lead to incorrect reduced mobility values (and hence CCS). Low pressure IMS systems do not generally exhibit such mobility shifts because the buffer gas composition is well controlled and ions are well desolvated.

The understanding that fentanyls exhibit two gas-phase protomers begs the question of whether other NSOs, like nitazenes, also exhibit two or more IMS distributions that are possibly protomers. Ideally this information could be used as a diagnostic indicator that NSOs are present in a sample. However, it is known that other drug compounds besides NSOs exhibit two IMS distributions, including antibiotics like fluoroquinolones (e.g., cefpodoxime, ciprofloxacin, enoxacin, norfloxacin, pefloxacin, sarafloxacin) and ampicillins (e.g., bacampicillin),[28] and topical anesthetics (benzocaine).[46] Since many different chemical compounds can exhibit two IMS distributions, there is a need to employ multimodal techniques, preferably high-resolution ones, to be able to distinguish between NSOs and other compounds in a generalizable manner.

This is where high-resolution hybrid measurements, like those from a recently developed SLIM-Orbitrap platform,[47] can play a critical role. Hollerbach et al. recently demonstrated the potential of SLIM-Orbitrap MS for finding novel chemical signatures of fentanyls.[22] The authors proposed their technology could be extended to find unique chemical signatures of other NSOs, and nitazenes are a logical extension from fentanyls since they are becoming increasingly prevalent and are concerning from a public health standpoint. In this study, the first IMS measurements on a set of fourteen nitazene analogs using a SLIM-Orbitrap platform are demonstrated and the first published CCS measurements of these nitazenes in positive ion mode are reported. The effect of water concentration on the signal intensities of the bimodal IMS distributions are discussed. Additionally, the bimodal IMS distributions are shown to produce different fragmentation patterns, suggesting that nitazenes also exhibit gas-phase protomers. Furthermore, the cyclic capability of the high-resolution SLIM was used to partially separate four groups of nitazene isomers, showcasing the first IMS separations of very similar nitazene isomers. A discussion is given on how the findings on nitazenes and fentanyls can be used to identify their presence in a mixture and how this information might be used to predict whether future NSOs can be found without requiring authentic reference standards for final validation.

Experimental Details

Chemicals

Nitazene and thirteen nitazene analogs (collectively termed nitazenes) were purchased from either Cayman Chemical (Ann Arbor, MI, USA) or Cerilliant (Round Rock, TX, USA); Drug

Enforcement Agency (DEA) scheduled compounds were purchased as exempt preparations at concentrations of 100 μg/mL or 1 mg/mL in methanol. The fourteen nitazenes were: (1) nitazene, (2) metodesnitazene, (3) protodesnitazene, (4) isotodesnitazene, (5) 5-methyl etodesnitazene, (6) ethyleneoxynitazene, (7) N-piperidinyl metonitazene, (8) N-pyrrolidino etonitazene, (9) etonitazene, (10) protonitazene, (11) isotonitazene, (12) butonitazene, (13) isobutonitazene, and (14) secbutonitazene. The chemical structures of the fourteen nitazenes are provided in the Supporting Information (Figure S2). MarvinSketch was used for drawing and displaying the chemical structures of nitazene and all nitazene analogs (Marvin 24.1.1, 2024, ChemAxon (http://www.chemaxon.com)). Four sets of nitazene analogs were isomers: (1) protonitazene, isotonitazene, (2) protodesnitazene, isotodesnitazene, 5-methyl etodesnitazene, (3) butonitazene, isobutonitazene, secbutonitazene, (4) ethyleneoxynitazene, N-piperidinyl metonitazene, N-pyrrolidino etonitazene. Five tetraalkylammonium salts (TAAs: butyl-, pentyl-, hexyl-, heptyl-, octyl- denoted as C4 – C8, respectively) were purchased from Sigma-Aldrich (St. Louis, MO, USA) and prepared at 1 μM equimolar concentration for use as internal CCS calibrants. Mixtures of nitazene and nitazene analogs were prepared at 1 μM equimolar concentration in ACS-grade methanol or 1:1 methanol:water (ultrapure water from a MilliQ water dispensing system).

Instrumentation

All HR-IM-MS/MS experiments were performed using a previously described dual-gated SLIM-Orbitrap platform operating in positive ion mode.[47] Briefly, the SLIM-Orbitrap is composed of an 11-meter path length SLIM coupled to a Q-Exactive Plus Orbitrap MS (Thermo-Fisher, Waltham, MA, USA). The dual-gated scanning technique[48] is used to couple the SLIM to the Orbitrap, which allows the system to simultaneously perform IM separations over 11 meters, mass analysis using the Orbitrap's highest mass resolution setting (140k), and higher-energy collision-induced dissociation (HCD). Nitrogen was used as the buffer gas for the SLIM (2.2-2.3 Torr) and the Orbitrap HCD cell (pressure automatically adjusted based on instrument conditions). All HCD experiments were performed using normalized collision energies (NCE = 30 eV). The Orbitrap was calibrated using Pierce LTQ Velos ESI positive ion calibration solution (Thermo-Fisher, Waltham, MA, USA) immediately prior to all experiments. All solutions were directly infused at 0.75 μL/min using an HF-etched fused-silica nanoelectrospray emitter (20 μm o.d.) and a syringe pump (Harvard Apparatus, Holliston, MA, USA).[49]

Signal processing and data analysis

Data were acquired as .RAW files by the Orbitrap, converted to .mzXML files using the 'MSConvert' tool from ProteoWizard,[50] and then imported into Matlab (Mathworks, Natick, MA, USA) for data processing and plotting. All extracted IM spectra were taken over *m/z* windows of ±0.005 amu. Mass errors (Δmmu) were calculated using XCalibur software.

Results and Discussion

High-resolution IMS-MS of nitazene and nitazene analogs in positive ion mode

Extracted ion mobilograms (XIMs) of the seven different groups of nitazene isomers were generated using a ± 0.005 *m/z* window, and the results are shown in Figure 1. The XIMs represent *m/z* 338 (metodesnitazene), *m/z* 353 (nitazene), *m/z* 366 (protodesnitazene/isotodesnitazene/5-methyl etodesnitazene), *m/z* 395 (ethyleneoxynitazene/N-piperidinyl metonitazene/N-pyrrolidino etonitazene), 397 (etonitazene), 411 (protonitazene/isotonitazene), and 425 (butonitazene/isobutonitazene/secbutonitazene). All nitazenes existed as the protonated forms. The XIMs showed that all nitazenes exhibited two primary IM distributions. This includes the three non-isobaric nitazenes (*m/z* 338, 353, 397) that were present in the mixtiure as well as the four groups of isobaric nitazenes (*m/z* 366, 395, 411, 425). Furthermore, the intensities of the first IM distribution compared to the second IM distribution differed depending on the nitazene. The first IM distributions of *m/z* 338 (Figure 1A – red plot) and *m/z* 366 (Figure 1C – blue plot) exhibited lower intensities than the second IM distributions. However, the first IM distributions of *m/z* 353, 395, 397, 411, and 425 exhibited higher intensities than the second IM distributions. Note that metodesnitazene (*m/z* 338) and the three nitazenes with *m/z* 366 do not possess nitro groups at the R1 position, whereas the other five nitazene groups do possess a nitro group at the R1 position. It is possible this nitro group contributes to the solution-phase or gas-phase structure adopted by the nitazenes. *m/z* 338 also exhibited a third IM distribution that was low intensity and lower mobility than the other two IM distributions. No third distribution was observed for *m/z* 366, so this third peak was a unique feature for metodesnitazene out of the fourteen nitazenes evaluated in this study. However, it is possible that experiments using higher concentrations of nitazenes would improve the signal intensities of any undetected peaks for the other nitazenes.

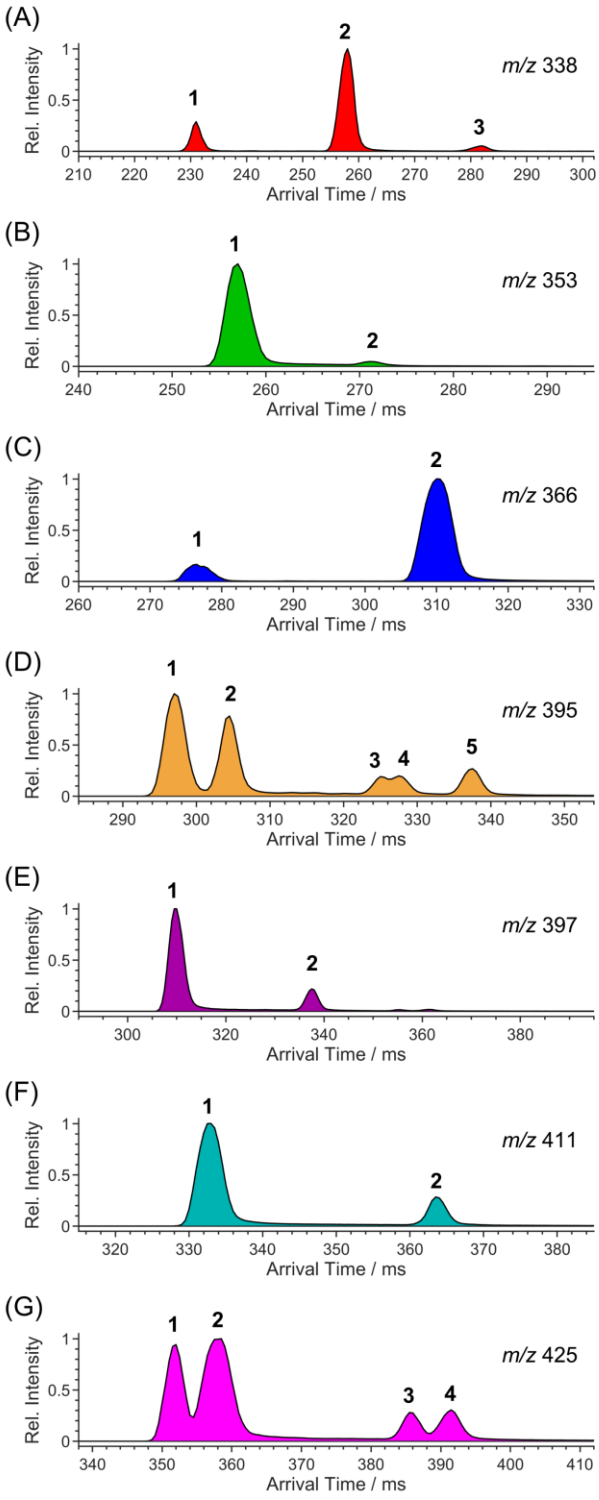

Figure 1: Extracted SLIM ion mobilograms of a 1 μM equimolar mixture of fourteen nitazenes in methanol from an 11-meter SLIM separation. (A) *m/z* 338 - metodesnitazene, (B) *m/z* 353 - nitazene, (C) *m/z* 366 - protodesnitazene / isotodesnitazene / 5-methyl etodesnitazene, (D) *m/z* 395 - ethyleneoxynitazene / N-piperidinyl metonitazene / N-pyrrolidino etonitazene, (E) *m/z* 397 - etonitazene, (F) *m/z* 411 - protonitazene / isotonitazene, (G) *m/z* 425 - butonitazene /

isobutonitazene / secbutonitazene. Positive ion mode. SLIM pressure = 2.28 Torr nitrogen. In-SLIM accumulation time = 20 ms. TW = 112 m/s sine waves at 17.5 $V_{0\text{-}p}$. Guard = +10 V_{dc}. Dual-gate = 1.0 ms width, 0.5 ms / step. Scans per Δt = 10. Orbitrap mass resolution setting = 140k.

The XIMs corresponding to the groups of isomers (*m/z* 366, 395, 411, 425) contained more peaks than the XIMs of the non-isobaric nitazenes. The XIM of *m/z* 366 (Figure 1C - blue plot) was expected to show three distinct ion distributions corresponding to three isomers (protodesnitazene/isotodesnitazene/5-methyl etodesnitazene). However, only two IM distributions were observed. Since this experiment was performed on a mixture of the three isomers and not individual compounds, it is expected that the three nitazene isomers each exhibited two IM distributions, but the first and second IM distributions of all three nitazenes completely overlapped in the 11-meter SLIM separation. This was not entirely unexpected since the structural differences between these three isomers are small. The only structural difference between protodesnitazene and isotodesnitazene is the presence of an N-propoxy group (R-O-$CH_2CH_2CH_3$) or isopropoxy (R-O-$CH(CH_3)_2$) group, respectively, in the R4 position (see Supporting Information Figure S1 and Figure S2). It is expected that this structural difference would only contribute to a small change in CCS. On the other hand, 5-methyl etodesnitazene possesses a more prominent structural difference in that an N-ethoxy group (R-O-CH_2CH_3) is present at the R4 position, but an additional methyl group is present at the R1 position. A methyl group shift to the R1 position might be expected to contribute to a greater CCS change than changing from a propoxy group to an isopropoxy group at R4. However, among the three nitazene isomers with *m/z* 366, the presence of methyl groups in different positions in the nitazene structure did not induce large enough CCS shifts to observe the expected six ion distributions in the 11-meter SLIM separation.

The 11-meter SLIM separation also did not differentiate the two nitazene isomers with *m/z* 411 (Figure 1F – aquamarine plot), which corresponded to protonitazene and isotonitazene. Protonitazene and isotonitazene also possess the same small structural differences of an N-propoxy group and an isopropoxy group at the R4 position, respectively. However, protonitazene and isotonitazene both have nitro groups at the R1 position, whereas the three nitazenes with *m/z* 366 either possess a methyl group or no functional group at the R1 position. The presence of a nitro group for *m/z* 411 compounds appears to have contributed to the observation that the higher mobility IM distribution exhibited greater intensity than the lower IM distribution. But since all nitazenes in this study exhibited two IMS distributions, the presence of a nitro-group substituent

at the R1 position must not be necessary for nitazenes to exhibit two IM distributions. Rather, the nitro group at the R1 position only seems to affect the intensity ratio of the two IM distributions. This information also suggests that the two IM distributions exhibited by nitazenes do not require protonation at the nitro group, otherwise one of the IM distributions would be absent. The lack of protonation at the nitro group may not be entirely surprising as other nitro-containing compounds, like explosives, are not known to exhibit protonation at the nitro group.[51]

While the 11-meter SLIM separations for *m/z* 366 and *m/z* 411 did not indicate that more than one compound was present (even though more than one compound was indeed present for both *m/z* groups), the nitazene isomer groups with *m/z* 395 (Figure 1D – orange plot) and *m/z* 425 (Figure 1G – pink plot) exhibited enough of an IMS separation to indicate that more than one compound was present. For example, the XIM of *m/z* 395 showed five high intensity IM distributions instead of just two. Two of the IM distributions possessed higher intensities and higher mobilities (i.e., shorter arrival times) than the other three IM distributions, which suggests more than one nitazene was present. While the two higher mobility IM distributions (Figure 1D - peaks 1 and 2) were baseline resolved, only one of the lower mobility IM distributions (Figure 1D - peak 5) was baseline resolved from the other two. The other two lower IM distributions (Figure 1D - peaks 3 and 4) were only partially resolved. However, the benefit of analyzing a class of compounds that exhibits two IM distributions is that only one of the groups of IM distributions (either high mobility or low mobility) needs to show an indication that more than one compound exists, not both. While two IM distributions were present in the high mobility group, there were three IM distributions in the low mobility group. Logically this means that three compounds with *m/z* 395 must be present, and indeed there were three compounds comprising *m/z* 395 (ethyleneoxynitazene/N-piperidinyl metonitazene/N-pyrrolidino etonitazene). The question of which IM distribution corresponded to which nitazene can be addressed by performing mobility-selected MS/MS (as opposed to analyzing samples containing the individual nitazenes), which is discussed later. However, it is much more desirable to confirm the identify of an unknown nitazene based solely on experimental data without requiring reference material (i.e., reference-free), since emerging NSOs will probably not have readily available standards to compare to.

The same logic can be applied to the group of three nitazenes with *m/z* 425 (Figure 1G – pink plot). This XIM also shows two IM distributions with higher intensities and higher mobilities

(i.e., shorter arrival times) than the lower IM distributions, but there were only two lower IM distributions (Figure 1G – peaks 3 and 4) instead of three. While this XIM doesn't clearly indicate that three nitazenes were present, it was apparent that the second higher mobility IM distribution (Figure 1G – peak 2) was wider than the first higher mobility IM distribution (Figure 1G - peak 1) by ~ 2 ms. The broadness of this peak suggests that more than one nitazene could be present, but an 11-meter SLIM separation was not enough to resolve them. SLIM separations employing longer path lengths would be needed to at least partially resolve these compounds, and the results of such experiments are presented later.

To date, there have not been any published reports of the CCS of nitazenes, and thus CCS values from this study using an 11-meter SLIM separation are reported. The mixtures of nitazenes also contained five TAA cations (*m/z* 242, 298, 354, 410, 466) which were used as internal calibrants. An IMS calibration plot of reduced CCS was first generated for the fourteen nitazenes and is shown in the Supporting Information along with a 95% confidence band (Figure S3) and a table containing the $^{TW}CCS_{N2}$ values of the nitazenes are given in Table S1. This table also contains other analytical metrics from the HR-IMS-MS experiments, including exact mass measurements from the Orbitrap, mass error relative to predicted molecular formula, Orbitrap mass resolution of the monoisotopic mass (Δppm), peak center from SLIM separation, fwhm of the peaks from the SLIM separation, and $^{TW}CCS_{N2}$-based resolving power. The CCS-based resolving power of each IM distribution was calculated using equation (1):

$$R_p = \frac{CCS}{\Delta CCS} \quad (1)$$

where CCS and ΔCCS are the peak center and full width at half maximum (fwhm), respectively, in the CCS domain. Note that the table includes experimentally measured values for both IM distributions of the nitazenes. The average Rp^{CCS} obtained for the protonated nitazenes was 167.

Note that the total analysis time for the nitazene mixture was ~14 minutes when only acquiring one mass spectrum per dual-gated time step and using 500 µs time steps. However, these first 11-meter SLIM experiments were performed using an average of ten IMS separations per dual-gated time step, meaning the entire experiment took ~140 minutes. A snapshot of the raw data from this experiment from XCalibur is shown in the Supporting Information (Figure S4). This slow analysis speed currently prevents coupling online LC with the SLIM-Orbitrap. However, it

is possible to gain the benefits of LC separations (e.g., reduced competitive ionization) by performing LC fractionation and analyzing the fractions individually with the SLIM-Orbitrap.

Influence of water on IM distributions

Since all fourteen nitazenes exhibited at least two IM distributions, an explorative study was performed to determine the cause of these two peaks, such as them being rotational conformers (rotomers), protonation site specific conformers (protomers), or another type of gas-phase conformer. In a previous study involving fentanyl and fentanyl analogs, Hollerbach et al. examined how the concentration of water in the ESI solvent affected the IMS distributions and noticed large differences in the intensity ratios of the two IM distributions that all fentanyls exhibited. The same logic was used in this study and prepared the fourteen nitazenes (and five TAAs) in a mixture of 1:1 methanol:water. The concentrations were equimolar at 1 μM.

XIMs of the same groups of nitazenes in 1:1 methanol:water acquired after an 11-meter SLIM-Orbitrap separation are shown in Figure 2. The largest changes in signal intensities occurred for the nitazenes corresponding to *m/z* 338 and *m/z* 366 (Figure 2A and Figure 2C). The XIMs of these nitazene groups showed that water caused the highest mobility IM distribution to become more intense than the lower mobility IM distribution(s), whereas the lower mobility distributions exhibited greater intensity when no water was present (see Figure 1). This change was much more prominent than for the other five XIMs, which showed that water caused the signal intensities of the lower IM distributions to decrease slightly compared to the signal intensities of the higher mobility distributions. It was also observed that the two groups of nitazenes whose two IM distributions exhibited large signal intensity changes due to the presence of water all lacked a nitro group at the R1 position (see Figure S2 – *m/z* 366). The other groups of nitazenes that did not exhibit such large signal intensity changes all possessed a nitro group at the R1 position. This finding suggests that nitro groups in nitazenes play a crucial role in the emergence of IM distributions and could potentially be used to compliment an exact mass measurement (leading to chemical formula) to determine whether an unknown nitazene contains a nitro group.

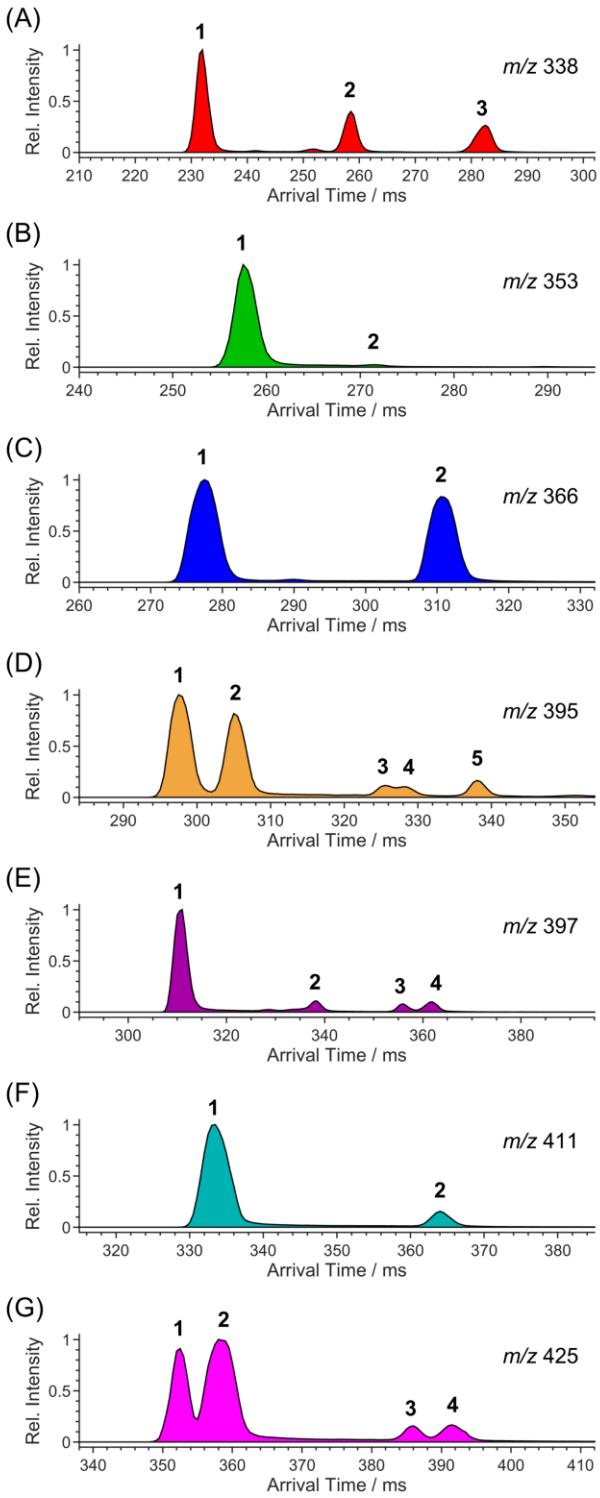

Figure 2: Extracted SLIM ion mobilograms of a 1 μM equimolar mixture of fourteen nitazenes in 1:1 water:methanol from an 11-meter SLIM separation. (A) *m/z* 338 - metodesnitazene, (B) *m/z* 353 - nitazene, (C) *m/z* 366 - protodesnitazene / isotodesnitazene / 5-methyl etodesnitazene, (D) *m/z* 395 - ethyleneoxynitazene / N-piperidinyl metonitazene / N-pyrrolidino etonitazene, (E) *m/z* 397 - etonitazene, (F) *m/z* 411 - protonitazene / isotonitazene, (G) *m/z* 425 - butonitazene /

isobutonitazene / secbutonitazene. Positive ion mode. SLIM pressure = 2.28 Torr nitrogen. In-SLIM accumulation time = 20 ms. TW = 112 m/s sine waves at 17.5 $V_{0\text{-}p}$. Guard = +10 V_{dc}. Dual-gate = 1.0 ms width, 0.5 ms / step. Scans per Δt = 10. Orbitrap mass resolution setting = 140k.

It is not entirely unexpected that the intensities of the two IM distributions of nitazenes depends on the presence of water in the ESI solvent, though the extent to which a nitro group affects the signal intensities of the two IM distributions was surprising. Hollerbach et al. recently demonstrated that fentanyls (fentanyl + fentanyl analogs) also exhibit two gas-phase protomers whose two IM distributions depend on the water concentration in the ESI solvent. However, previously observations showed that water caused the second IM distributions of fentanyls to exhibit higher signal intensities compared to the first. This is the opposite of what this study found for nitazenes, which is that water caused the first IM distributions of nitazenes to exhibit higher signal intensities. Nitazenes and fentanyls are structurally different and thus it is not unexpected that they exhibit different behaviors in the presence of water. In separate but related work, Warnke et al. demonstrated that benzocaine also exhibits two IM separable distributions, and that water causes the higher mobility distribution to exhibit higher intensity than the lower mobility distribution.[46] The solvent study presented here shows that nitazenes exhibit behavior closer to benzocaine than fentanyl. Warnke et al. also used density functional theory (DFT) and IR-vibrational spectroscopy to confirm that the two IM distributions of benzocaine were caused by protonation at the amino and carbonyl sites, and therefore the two IM distributions are gas-phase protomers whose protonation sites strongly depend on the electric properties of the solvent medium. Since the lower mobility distributions of all the nitazenes analyzed in this study also exhibited lower signal intensities when water was present in the ESI solvent, this is experimental evidence that supports that nitazenes also exhibit gas-phase protomers, similar to benzocaine and fentanyl. These observations should be considered when using IMS to analyze solutions that potentially contain both opioid classes because having the ability to readily observe two IM distributions is useful for differentiating fentanyls and nitazenes from other compounds that might coexist in solution. It is proposed to use less water in the ESI solvent when analyzing nitazenes to ensure that both IM distributions can be observed.

MS/MS of mobility-selected nitazene distributions

To further study the nature of the multiple IM distributions exhibited by all fourteen nitazenes, MS/MS was performed on the individual IM distributions. The dual-gate of SLIM was

used to mobility-select an IM distribution from an HR-IMS separation, and the Orbitrap was used to mass-select a narrow *m/z* window (± 0.5 *m/z*) for HR-MS/MS in the HCD cell (NCE = 30 eV).

Mobility and mass-selected HR-MS/MS spectra of the first and second IM distributions of nitazenes with *m/z* 338, *m/z* 353, *m/z* 366, *m/z* 397, and *m/z* 411 are given in Figure 3. The MS/MS spectra of the first and second IM distributions are shown on the top and bottom plots, respectively. These five *m/z* groups (eight nitazenes in total) were plotted together because their IMS spectra only displayed two IM distributions even though multiple nitazene isomers were present. The first and second IM distributions of all five nitazene groups also displayed different MS/MS spectra. The first IM distributions produced two high intensity fragment ions with *m/z* 72 and *m/z* 100, one low intensity fragment ion between *m/z* 100-150, and one or more low intensity fragment ions between *m/z* 260-300. However, the second IM distributions of all nitazenes in these groups only produced fragment ions with *m/z* 72 and *m/z* 100. The shared fragment ions from both IMS distributions all possessed the same exact mass, but this study does not have evidence to support the existence of fragment ion isomers. The difference in fragmentation spectra of the two IM distributions of all nitazenes could be indicative of protomers, which are known to exhibit multiple IM distributions that produce different fragmentation patterns. Fentanyls, benzocaine, and para-aminobenzoic acid are known (or expected) to exhibit two IM distributions that produce different fragmentation patterns and change intensities depending on the amount of water in the ESI solvent.[22,46] Since nitazenes exhibit similar behavior, it seems likely that they also exhibit gas-phase protomers. A logical next step is to perform density functional theory (DFT) calculations and place a proton at different basic residues to see if the 3D gas-phase chemical structures differ.

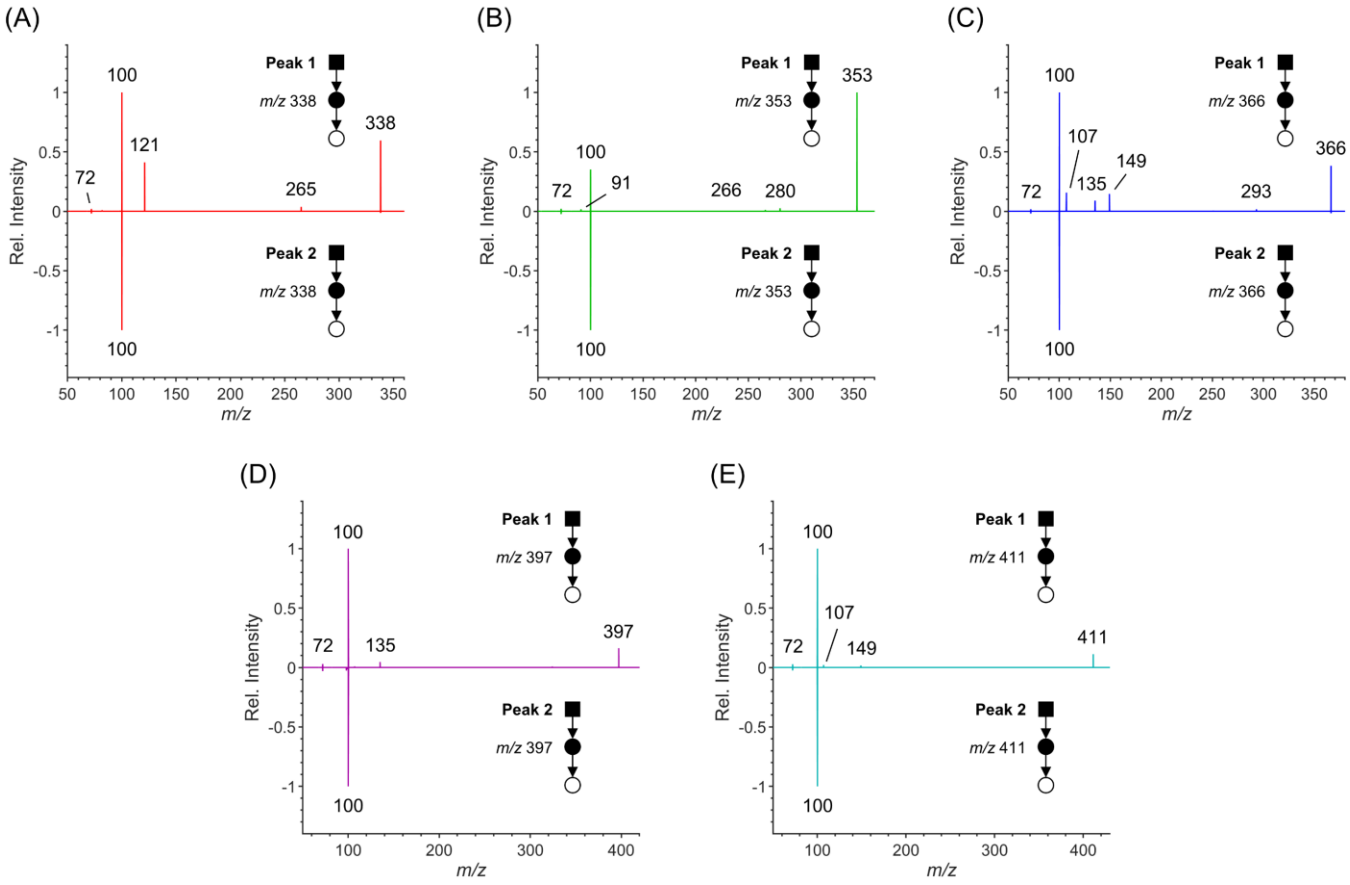

Figure 3: MS/MS spectra of the (top) higher mobility IM distributions and (bottom) lower mobility IM distributions of (A) *m/z* 338 - metodesnitazene, (B) *m/z* 353 - nitazene, (C) */z* 366 - protodesnitazene / isotodesnitazene / 5-methyl etodesnitazene, (D) *m/z* 397 - etonitazene, (E) *m/z* 411 - protonitazene / isotonitazene. Positive ion mode. SLIM pressure = 2.27 Torr nitrogen. In-SLIM accumulation time = 20 ms. TW = 112 m/s sine waves at 17.5 $V_{0\text{-}p}$. Guard = +10 V_{dc}. Dual-gate = 1.0 ms width, 1.0 ms / step. Scans per Δt = 10. Orbitrap mass resolution setting = 140k. HCD normalized collision energy = 30 eV. Concentration = 1 µM in methanol.

It would be useful to determine which potential protonation sites are the most likely before performing DFT calculations. It is proposed that this can be done by a process of elimination based on the data in this study. First, the experimental results of the groups of nitazenes were used to determine where protonation likely does not occur. The nitro group was ruled out because four of the nitazenes in this study did not possess a nitro group, yet they still produced two IM distributions. The ether oxygen was also ruled out as a protonation site because one of the nitazenes in this study did not contain an ether group at the R4 position (nitazene itself), yet it also exhibited two IM distributions. Therefore, there are logically only three places where protonation can occur: (1) the N1 position on the benzimidazole ring, (2) the N3 position on the benzimidazole ring, and (3) the nitrogen on the triethylamine. The eight nitazenes in the five *m/z* groups shown

in Figure 3 all possessed triethylamine functional groups at the R2/R3 positions, and it may seem reasonable to place a proton on this trisubstituted amine group. However, the presence of fragment ions with *m/z* 72 and *m/z* 100 would not be formed from protonation at the triethylamine group. Rather, protonating the triethylamine and cleaving the bond between the nitrogen and carbon connected to the benzimidazole ring would produce a neutral loss of *m/z* 73. Indeed, neutral losses of 73 were observed in the first IM distributions of all five nitazene groups, albeit with low signal intensities. Fragment ions corresponding to a neutral losses of 73 are *m/z* 265 (for *m/z* 338), *m/z* 280 (for *m/z* 353), *m/z* 293 (for *m/z* 366), *m/z* 224 (for *m/z* 397), and *m/z* 338 (for *m/z* 411). However, if protonation occurs at the N1 position on the benzimidazole ring, a bond cleavage at the carbon-nitrogen bond of the triethylamine would produce a fragment ion with *m/z* 72 (N,N-diethylamine cation), and a bond cleavage at the carbon-nitrogen of the benzimidazole ring would produce a fragment ion with *m/z* 100 (triethylamine cation). Both fragment ions are readily observed in all instances, and since the eight nitazenes in this group possessed a triethylamine, *m/z* 72 and *m/z* 100 are expected to be shared fragments.

It is not entirely clear why both the high and low mobility IM distributions produce *m/z* 72 and *m/z* 100 fragment ions. The first IM distributions also show low intensity fragment ions corresponding to a carbon-carbon bond cleavage between the benzimidazole ring and the benzyl ring. These fragment ions are *m/z* 121 (for *m/z* 338), *m/z* 91 (for *m/z* 353), *m/z* 135 and *m/z* 149 (for *m/z* 366), *m/z* 135 (for *m/z* 397), and *m/z* 149 (for *m/z* 411). If protonation occurs at one of the benzimidazole nitrogens, any mechanism that supports the cleavage of the carbon-carbon bond between the benzimidazole and benzyl ring could be assigned one of the IM distributions. It is currently not clear which nitrogen would most likely produce this bond cleavage, but logically the formation of only *m/z* 72 and *m/z* 100 seems supported by protonating N1 on the benzimidazole ring. Based on these findings and logic, it is proposed that the two IM distributions of nitazenes are comprised of at least two gas-phase protomers and not some other gas-phase conformations. Furthermore, it is proposed that the protonation site of the second IM distributions of nitazenes is at the N1 position on the benzimidazole ring. This is because the second IM distributions of all nitazenes only produced fragments with *m/z* 72 and *m/z* 100. Therefore, it is hypothesized that the protonation site of the first IM distributions of nitazenes is on the N3 position of the benzimidazole ring. However, note that a third gas-phase protomer could exist via protonation at the triethylamine nitrogen, which would result in a neutral loss of *m/z* 73. Since these neutral losses only occurred

for the first IM distributions, it is possible that the two protomers exhibit similar CCSs that could not be separated with an 11-meter SLIM. This hypothesis would be greatly supported by structural prediction work and rigorous electron pushing mechanisms for fragmentation.

Additionally, precursor *m/z* 366 also showed the presence of *m/z* 135 and *m/z* 149 fragment ions. This makes sense because three nitazene isomers possessed *m/z* 366, and therefore at least one of the fragment ions corresponded to one of the nitazenes and represents an instance where the MS can differentiate between two or more compounds while an 11-meter SLIM separation cannot. Comparing to the chemical structures in Figure S2 and using the knowledge of where the bonds cleave, the *m/z* 135 fragment ion originated from 5-methyl etodesnitazene while *m/z* 149 originated from protodesnitazene and isotodesnitazene. Fragment ion *m/z* 107 had a chemical formula of C_7H_7O (0.549 Δppm), and since the three nitazene isomers with *m/z* 366 only have an ether oxygen, this fragment must correspond to a benzyl ring with ether oxygen but a loss of the alkyl functional groups from the ether. This is also supported by the fact that nitazene does not have an ether at the R4 position and does not produce a fragment ion with *m/z* 107. These data show that the MS/MS spectra of nitazenes can be used to inform if multiple isomeric nitazenes are present. This knowledge can then be used to decide whether performing extended IMS separations to further validate the presence of multiple isomers would be useful.

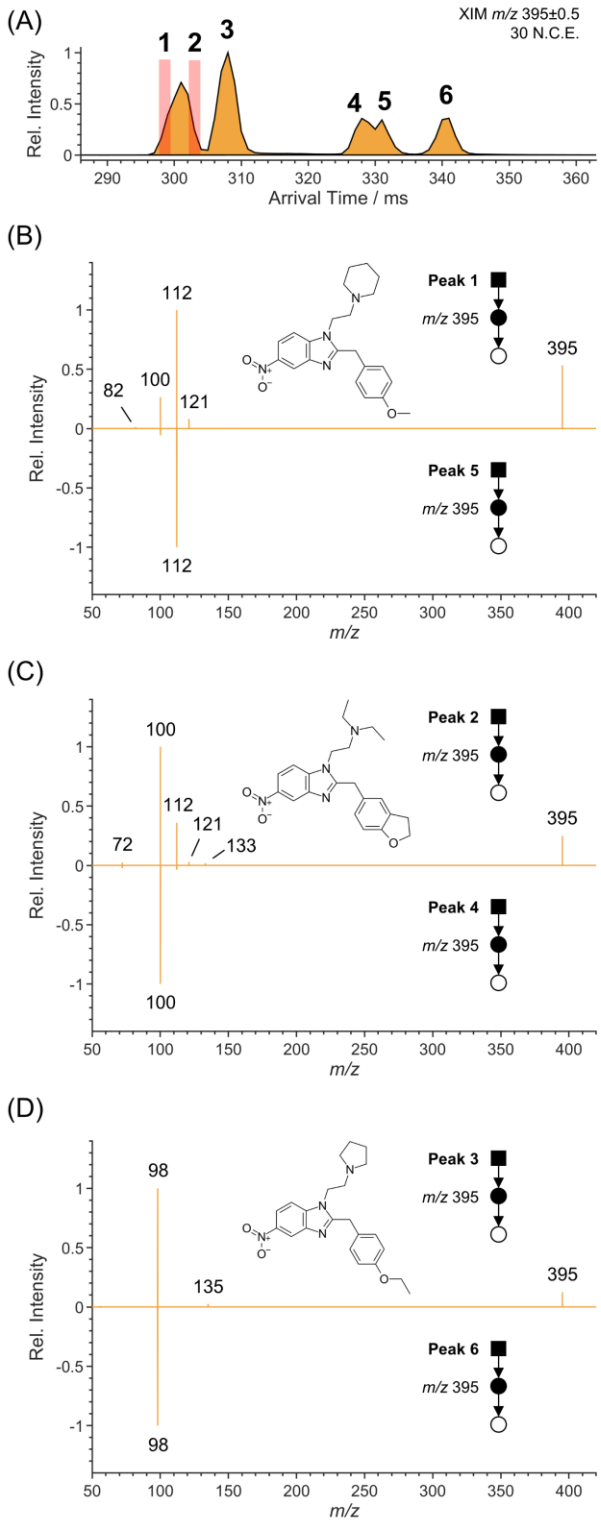

Figure 4: (A) SLIM IMS spectrum of *m/z* 395. (B) MS/MS spectra of peak 1 (top) and peak 5 (bottom). (C) MS/MS spectra of peak 2 (top) and peak 4 (bottom). (D) MS/MS spectra of peak 3 (top) and peak 6 (top). Positive ion mode. SLIM pressure = 2.27 Torr nitrogen. In-SLIM accumulation time = 20 ms. TW = 112 m/s sine waves at 17.5 $V_{0\text{-}p}$. Guard = +10 V_{dc}. Dual-gate

= 1.0 ms width, 1.0 ms / step. Scans per Δt = 10. Orbitrap mass resolution setting = 140k. HCD normalized collision energy = 30 eV. Concentration = 1 µM in methanol.

While the MS/MS of the eight nitazenes in Figure 3 indicate that they possess triethylamine groups, nitazenes that do not possess a triethylamine functional group will not necessarily produce a neutral loss of 73 or fragment ions of *m/z* 72 and *m/z* 100. Instead, the neutral loss and fragment ions would be dependent on which functional group is present. Such differences can be seen in the MS/MS spectra of the three nitazene isomers comprising *m/z* 395, which are shown in Figure 4. Two of these nitazene isomers (N-piperidinyl metonitazene/N-pyrrolidino etonitazene) possess ethyl-ring structures instead of a triethylamine group, while the third nitazene isomer (ethyleneoxynitazene) does possess a triethylamine. Note that two MS/MS spectra were generated from the front and rear of IM distribution 1 (Figure 4B – top MS/MS spectrum, Figure 4C – top MS/MS spectrum) while the other four MS/MS spectra were generated from the other four mobility resolved IM distributions (Figure 4B – bottom MS/MS spectrum, Figure 4C – bottom MS/MS spectrum, Figure 4D – top and bottom MS/MS spectra). The group of MS/MS spectra from *m/z* 395 showed three high intensity fragments: *m/z* 112, *m/z* 100, and *m/z* 98. These fragment ions were present in both the high mobility IM distributions (Figure 4A - peaks 1,2,3) and low mobility IM distributions (Figure 4A – peaks 4,5,6). Based on previous knowledge, the *m/z* 100 fragment ion can be assigned to any nitazene possessing a triethylamine (assuming different functional groups produce fragment ions with different *m/z*). Ethyleneoxynitazene is the only compound in this group of nitazene isomers to possess a triethylamine, and peaks 2 and 4 are the only peaks that exhibit *m/z* 100. However, the presence of ethyl-ring structures from the other two nitazenes results in different fragment ions. N-piperidinyl metonitazene possesses an ethyl-piperidine ring, and cleavage at the ethyl carbon-piperidine nitrogen bond produces a fragment with *m/z* 112. Peak 1 and peak 5 both exhibit this fragment ion and therefore must represent N-piperidinyl metonitazene. By process of elimination, this means that peaks 3 and 6 are N-pyrrolidino etonitazene. However, peaks 3 and 6 also uniquely exhibit a fragment ion with *m/z* 98, which is formed by cleaving the bond between the ethyl carbon and pyrrolidine nitrogen. These data showed that even though the high mobility IM distributions of two nitazene isomers overlap, it was possible to identify that three nitazene isomers possessing *m/z* 395 were present by observing that three corresponding low mobility IM distributions, and that the highest mobility IM

distribution (peak 1,2) showed two different high intensity fragment ions. This demonstrates the power of using multimodal HR techniques for identifying nitazenes, even structural isomers.

However, identifying the correct number of nitazenes (and their chemical structures) becomes more complicated if the nitazene isomers exhibit identical MS/MS spectra, such as for butonitazene, isobutonitazene, and secbutonitazene. The MS/MS spectra of these three nitazene isomers (*m/z* 425) is shown in the Supporting Information (Figure S5). The two high mobility IM distributions produced fragment ions with *m/z* 72, *m/z* 100, *m/z* 352 (a low intensity neutral loss of 73), and *m/z* 107 while the two low mobility IM distributions only produced fragment ions with *m/z* 72 and *m/z* 100. As stated earlier, the broadness of peaks 2 and 4 suggests that more than one nitazene is present, but the 11-meter SLIM separation was insufficient to differentiate them. To determine the arrival time order of butonitazene, isobutonitazene, and secbutonitazene, the three compounds were analyzed individually. The XIMs of the three experiments and their sum are given in the Supporting Information (Figure S6). Secbutonitazene possessed the highest mobility, followed by isobutonitazene, and lastly n-butonitazene. Since emerging NSOs will likely not have readily available reference standards against which to compare experimental data, it is undesirable to analyze individual samples to determine arrival time (or other analytical metrics). This is where the cyclic capability of an IMS system like SLIM can provide crucial information.

Extended SLIM separations of structurally similar nitazene isomers

The SLIM-Orbitrap spectra discussed thus far could be used to differentiate between nine nitazenes, two groups of which contained three structural isomers each. Several isomers that were not differentiated by their exact mass or MS/MS spectra were successfully differentiated with the SLIM, and several isomers that were not separated with the SLIM were distinguished by their MS/MS spectra using the Orbitrap. However, the group of nitazene isomers containing butonitazene, isobutonitazene, and secbutonitazene were only partially differentiated with the SLIM and not differentiated at all with the Orbitrap. To determine if these three butyl-nitazene isomers and the other groups of nitazene isomers could be differentiated (*m/z* 366, *m/z* 395, *m/z* 411, *m/z* 425), the cyclic capabilities of the SLIM were used to perform extended IMS separations while simultaneously performing high resolution mass analysis with the Orbitrap.

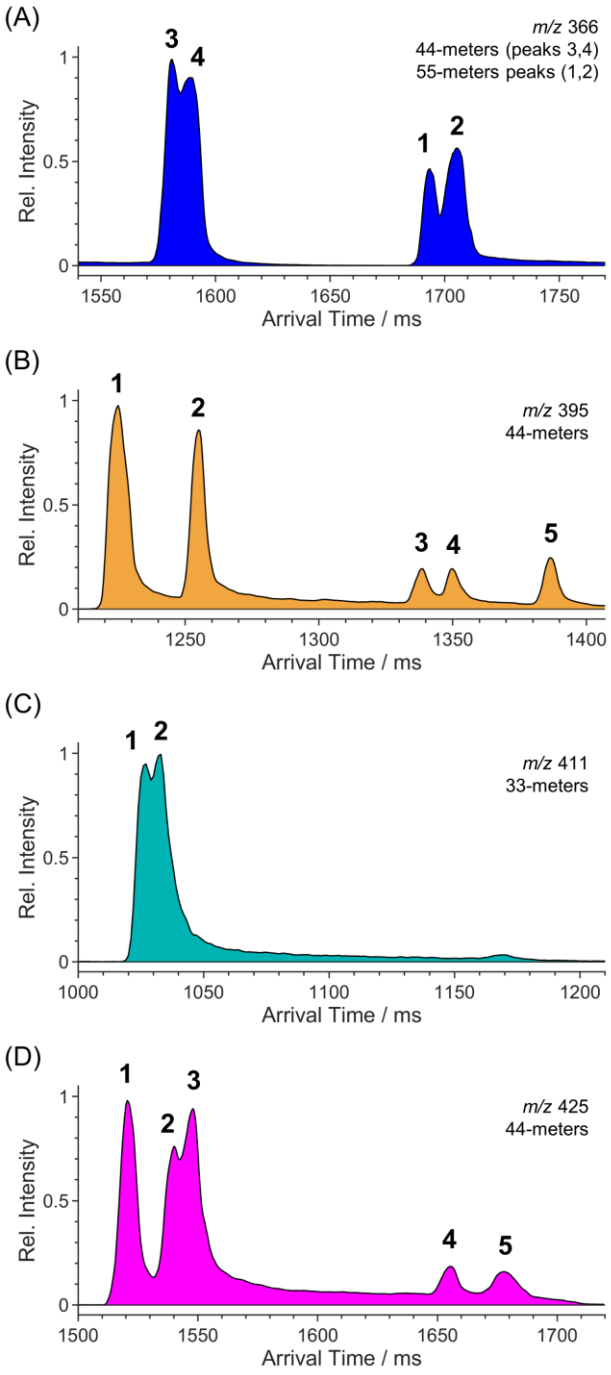

Figure 5: Extracted SLIM ion mobilograms of (A) *m/z* 366 - protodesnitazene / isotodesnitazene / 5-methyl etodesnitazene, (B) *m/z* 395 - ethyleneoxynitazene / N-piperidinyl metonitazene / N-pyrrolidino etonitazene, (C) *m/z* 411 - protonitazene / isotonitazene, and (D) *m/z* 425 - butonitazene / isobutonitazene / secbutonitazene acquired using 44/55-meters, 44-meters, 33-meters, and 44-meters of SLIM ion path length, respectively. Positive ion mode. SLIM pressure = 2.28 Torr nitrogen. In-SLIM accumulation time = 20 ms. TW = 112 m/s sine waves at 17.5 $V_{0\text{-}p}$. Guard = +10 V_{dc}. Dual-gate = 1.0 ms width, 0.5 ms / step. Scans per Δt = 10. Orbitrap mass resolution setting = 140k.

Four XIMs of the extended SLIM-Orbitrap IMS separations of the four nitazene isomer groups are shown in Figure 5. Separations were performed using 44-meters or 55-meters of IMS path length (4 or 5 total passes through the SLIM). After an extended IMS separation, the XIM of *m/z* 366 showed that the two previously observed high and low distributions each split into two partially resolved IM distributions. Note that intensities of the higher mobility distribution in the XIM of *m/z* 366 were higher than the lower IM distributions, which is opposite of what was observed when using 11-meters of IMS path length. This appears to be the result of ion lapping where the higher mobility IM distribution(s) traversed 55-meters while the lower mobility IM distributions traversed 44-meters. This means peaks 3 and 4 in Figure 5A represent an extended IMS separation of peak 2 in Figure 1C and Figure 2C, respectively, and peaks 1 and 2 in Figure 5A represent an extended IMS separation of peak 1 in Figure 1C and Figure 2C, respectively. Despite the ion lapping effect, the extra IMS separation resulted in partially resolved peaks where previously no indication was present. Peaks 3 and 1 in Figure 5A also appeared narrower than peaks 4 and 2. This suggests that another nitazene isomer was present under peaks 4 and 2. While it appears that more than 55-meters of SLIM separation path length will be needed to resolve all three nitazene isomers with *m/z* 366, this data suggests that full resolution will be possible with sufficient separation path length. Note that the 55-meter separation was the longest separation achievable using the current maximum Orbitrap injection time of 3 seconds per scan. It should be possible to achieve longer SLIM separations if the maximum Orbitrap injection time can be increased, or possibly if a new SLIM scan function is implemented to overcome the need to use the dual-gated ion injection method. A report on the latter will be presented in a subsequent study.

Alternatively, a 44-meter IMS separation resulted in near baseline-separation between peaks 3 and 4 of *m/z* 395, whereas they were previously only partially resolved in an 11-meter separation. Surprisingly, no additional separation between N-piperidinyl metonitazene and ethyleneoxynitazene (Figure 5B - peak 1) was observed with a 44-meter separation, indicating that further IMS separation is needed to resolve these two nitazene isomers. A 33-meter SLIM separation on protonitazene and isotonitazene (*m/z* 411) was also performed. The XIM of this extended IMS separation showed that the high mobility IM distribution began to separate into two partially resolved peaks (Figure 5C). The lower IM distribution only displayed one peak, and it was difficult to tell if additional separation would cause more than one peak to emerge. Based on the experiments where isobutonitazene exhibited a higher mobility than n-butonitazene, peak 1

was assigned to isotonitazene (isopropyl group) and peak 2 to protonitazene (n-propyl group). Both protonitazene and isotonitazene are known to be in circulation and are highly potent,[3] so being able to detect both in a mixture when using IMS is important. While this study only shows a partial separation between protonitazene and isotonitazene, it is believed even further extended IMS separations will fully resolve them.

Lastly, extended IMS separations on butonitazene, isobutonitazene, and secbutonitazene (*m/z* 425) were performed. The XIM of *m/z* 425 is shown in Figure 5D. As can be seen, the 44-meter IMS path length showed that peak 2 began to separate into two distinct IM distributions. Since these three peaks exhibit the same exact mass and MS/MS spectra, this added IMS separation is highly useful for indicating that multiple butyl nitazenes are present. As stated earlier, it is only necessary to have either the high or low mobility distributions exhibit an indication that nitazene isomers are present, not both. A good example of the high mobility IM distributions separating into three peaks while the low mobility IM distributions only display two peaks is given by *m/z* 425, and a good example of the low mobility IM distributions separating into three peaks while the high mobility IM distributions only display two peaks is given by *m/z* 395. However, the data show the utility of performing multimodal HR experiments on mixtures of nitazenes to separate structurally similar isomers. Unfortunately, even the SLIM-Orbitrap experiments utilizing extended IMS path lengths do not provide enough information to determine the arrival time order of butonitazene/isobutonitazene/secbutonitazene or protonitazene/isotonitazene without running individual samples. However, the data may be enough to determine which nitazene isomers are present, such as protonitazene and isotonitazene. The arrival time order of these two nitazenes could therefore be determined by employing computational modeling software to calculate their CCS, and this will inform on arrival time order.

Experimental evidence that nitazenes exhibit gas-phase protomers

Experiments were also performed to determine if nitazenes exhibit diagnostic gas-phase behavior, such as the formation of protomers, based on previous observations of similar behavior by fentanyl analogs.[22] The fourteen different nitazenes were all found to exhibit at least two IM separable distributions that produce different fragmentation spectra and change intensities when water is included or excluded from the ESI solvent. There does not appear to be any study where protonation sites are suggested for nitazenes (or that nitazenes exhibit two IM separable

distributions) and so this study tentatively proposes them. It was experimentally determined that the nitro groups and ether oxygens were not sites of protonation because four nitazenes did not possess a nitro group but still exhibited two IM distributions, and nitazene itself does not possess an ether group yet it still exhibited two IM distributions. This leaves three plausible protonation sites: (1) N1 on the benzimidazole ring, (2) N3 on the benzimidazole ring, and (3) the triethylamine nitrogen.

Since the MS/MS spectra of the second IM distributions of all nitazenes studied here only exhibited fragment ions corresponding to bond cleavages at the N1 benzimidazole nitrogen (e.g., fragments with *m/z* 100, *m/z* 98, *m/z* 112) or the ethyl-nitrogen (e.g., *m/z* 72) and no other detectable fragments, it is proposed that the lower mobility IM distribution of nitazenes is a protomer with protonation occurring at the N1 position on the benzimidazole ring. The higher mobility IM distributions of all nitazenes exhibited more fragments than the lower mobility IM distributions, including fragments from the same two bond cleavages, an additional fragment formed by cleaving between the C2 benzimidazole carbon and the benzyl ring, and a neutral loss of the triethylamine group. It seems that a neutral loss of 73 would most likely occur by protonating the triethylamine nitrogen and cleaving the carbon-nitrogen bond to form an N,N-diethylamine neutral. However, it does not appear that this would explain how fragmentation between the C2 benzimidazole carbon and benzyl ring occurs. Alternatively, this cleavage could be possible if the N3 nitrogen on the benzimidazole ring was protonated, followed by an electron pushing rearrangement. It is therefore proposed that the higher mobility IM distributions of nitazenes actually consist of two protomers: one with protonation occurring at the N3 position on the benzimidazole ring, and one with protonation occurring on the triethylamine nitrogen. It is recognized that this might not be an exhaustive list since more peaks emerged under different conditions, such as higher water concentrations in the ESI solvent. The presence of additional conformers (e.g., rotamers) could explain why other peaks emerged, or potentially why the extended SLIM separations showed peak tailing. It might be possible to separate the two possible protomers in the high mobility IM distributions by performing IMS separations using hundreds of meters of IMS separation path length. Such studies would provide interesting fundamental insights into the gas-phase behavior of nitazenes and could possibly be extended to other classes of drugs that might emerge as the opioid epidemic continues.

Conclusions

HR-IMS-MS/MS spectra of fourteen novel synthetic opioid nitazenes were acquired with a SLIM-Orbitrap platform. The spectra showed that each nitazene exhibited at least two IM separable distributions that produced different fragmentation patterns and changed intensities depending on the water concentration in the ESI solvent. The nitazenes lacking a nitro group exhibited the greatest shift in intensity. $^{TW}CCS_{N2}$ values for the fourteen nitazenes are also reported for positive ion mode. Furthermore, IMS separations over long IMS path lengths (>33 meters) showed at least partial separation between nitazene isomers that differed only in an alkyl group change (e.g., propyl / isopropyl or butyl/isobutyl/secbutyl) at the same functional group location. These experiments provide experimental evidence that nitazenes potentially exhibit three gas-phase protomers, with one of the protomers exhibiting a lower mobility than the other two protomers, which were indistinguishable by their mobility but were suggested by the fragmentation spectra.

While the HR-IMS-MS/MS data were sufficient to successfully differentiate nine of the nitazenes, including two groups of three isomers each, the data were insufficient to tell the arrival time order of the other groups of isomers. In the future, it would be highly desirable to use theoretical modeling methods (e.g., based on machine-learning or quantum chemistry) to predict the CCS values of these groups of nitazene isomers, which is how the arrival time order was determined in this study. The coupling of HR-IMS-MS/MS data with computational methods could potentially allow for nitazene identifications to be made in a reference-free approach. This methodology could also be applied to the analysis of other NSOs to expedite the determination of their chemical structure.

Associated Content

Supporting Information

Chemical structure of 2-benzylbenzimidazole (nitazene) backbone; chemical structures of fourteen nitazenes; snapshot of XCalibur display of nitazene separation using SLIM-Orbitrap; calibration curve with 95% confidence band; table of SLIM-Orbitrap measurements of a mixture of fourteen nitazenes and five tetraalkylammonium cations; XIM and MS/MS spectra of *m/z* 425; XIMs of individual butonitazene, isobutonitazene, and secbutonitazene samples.

Author Information

Corresponding Author

Adam L. Hollerbach - Biological Sciences Division, Pacific Northwest National Laboratory, Richland, Washington 99354, United States

Authors

Vivian S. Lin - Biological Sciences Division, Pacific Northwest National Laboratory, Richland, Washington 99354, United States

Yehia M. Ibrahim - Biological Sciences Division, Pacific Northwest National Laboratory, Richland, Washington 99354, United States

Robert G. Ewing - Nuclear, Chemistry & Biology Division, Pacific Northwest National Laboratory, Richland, Washington, 99354, United States

Thomas O. Metz - Biological Sciences Division, Pacific Northwest National Laboratory, Richland, Washington, 99354, United States

Kabrena E. Rodda - Nuclear, Chemistry & Biology Division, Pacific Northwest National Laboratory, Richland, Washington, 99354, United States

Notes

All authors declare no competing financial interest.

This research was supported by the PNNL Laboratory Directed Research and Development Program and is a contribution of the *m/q* initiative and the Strategic Investments Program. The *m/q* initiative supported the initial single-pass SLIM-Orbitrap experiments and manuscript preparation. The Strategic Investments Program supported the cyclic SLIM studies, including the characterization of new SLIM boards and the acquisition of the multipass SLIM data. This project was performed in the Environmental Molecular Sciences Laboratory, a DOE Office of Biological and Environmental Research sponsored national scientific user facility located on the PNNL campus. Battelle operates PNNL for the DOE under contract DE-AC05-76RLO01830.

References

(1) Spencer, M. R.; Gernett, M. F.; Miniño, A. M., Drug Overdose Deaths in the United States, 2002-2022, *NCHS Data Brief* **2024**, *491*.
(2) Tanz, L. J.; Gladden, R. M.; Dinwiddie, A. T.; Miller, K. D.; Broz, D.; Spector, E.; O'Donnell, J., Routes of Drug Use Among Drug Overdose Deaths - United States, 2020-2022, *MMWR Morb Mortal Wkly Rep* **2024**, *73*, 124-130.
(3) Walton, S. E.; Krotulski, A. J.; Logan, B. K. A Forward-Thinking Approach to Addressing the New Synthetic Opioid 2-Benzylbenzimidazole Nitazene Analogs by Liquid Chromatography–Tandem Quadrupole Mass Spectrometry (LC–QQQ-MS), *J. Anal. Toxicol.* **2021**, *46*, 221-231.
(4) Blanckaert, P.; Cannaert, A.; Van Uytfanghe, K.; Hulpia, F.; Deconinck, E.; Van Calenbergh, S.; Stove, C. Report on a novel emerging class of highly potent benzimidazole NPS opioids: Chemical and in vitro functional characterization of isotonitazene, *Drug Testing and Analysis* **2020**, *12*, 422-430.
(5) Janssen, P. A. J. A Review of the Chemical Features Associated with Strong Morphine-like Activity, *British Journal of Anaesthesia* **1962**, *34*, 260-268.
(6) Pergolizzi, J., Jr.; Raffa, R.; LeQuang, J. A. K.; Breve, F.; Varrassi, G. Old Drugs and New Challenges: A Narrative Review of Nitazenes, *Cureus* **2023**, *15*, e40736.
(7) Vandeputte, M. M.; Van Uytfanghe, K.; Layle, N. K.; St. Germaine, D. M.; Iula, D. M.; Stove, C. P. Synthesis, Chemical Characterization, and μ-Opioid Receptor Activity Assessment of the Emerging Group of "Nitazene" 2-Benzylbenzimidazole Synthetic Opioids, *ACS Chemical Neuroscience* **2021**, *12*, 1241-1251.
(8) Kimani, M. M.; Kern, S.; Lanzarotta, A.; Thatcher, M.; Lorenz, L. M.; Smith, S. W.; Collins, M.; Howe, G. W.; Wetherby Jr, A. E. Rapid screening of 2-benzylbenzimidazole nitazene analogs in suspect counterfeit tablets using Raman, SERS, DART-TD-MS, and FT-IR, *Drug Testing and Analysis* **2023**, *15*, 539-550.
(9) Hayes, K. L.; Lieberman, M. Assessment of two brands of fentanyl test strips with 251 synthetic opioids reveals "blind spots" in detection capabilities, *Harm Reduction Journal* **2023**, *20*, 175.
(10) Halifax, J. C.; Lim, L.; Ciccarone, D.; Lynch, K. L. Testing the test strips: laboratory performance of fentanyl test strips, *Harm Reduction Journal* **2024**, *21*, 14.
(11) Omar, J.; Slowikowski, B.; Guillou, C.; Reniero, F.; Holland, M.; Boix, A. Identification of new psychoactive substances (NPS) by Raman spectroscopy, *Journal of Raman Spectroscopy* **2019**, *50*, 41-51.
(12) Davidson, J. T.; Sasiene, Z. J.; Jackson, G. P. The influence of chemical modifications on the fragmentation behavior of fentanyl and fentanyl-related compounds in electrospray ionization tandem mass spectrometry, *Drug Testing and Analysis* **2020**, *12*, 957-967.
(13) Davidson, J. T.; Sasiene, Z. J.; Jackson, G. P. The characterization of isobaric product ions of fentanyl using multi-stage mass spectrometry, high-resolution mass spectrometry and isotopic labeling, *Drug Testing and Analysis* **2020**, *12*, 496-503.
(14) Mallette, J. R.; Casale, J. F.; Toske, S. G.; Hays, P. A. Characterization of (2R,4S)- and (2R,4R)-2-Methylfentanyl and their differentiation from cis- and trans-3-Methylfentanyl, *Forensic Chemistry* **2018**, *8*, 64-71.
(15) Nan, Q.; Hejian, W.; Ping, X.; Baohua, S.; Junbo, Z.; Hongxiao, D.; Huosheng, Q.; Fenyun, S.; Yan, S. Investigation of Fragmentation Pathways of Fentanyl Analogues and Novel Synthetic

Opioids by Electron Ionization High-Resolution Mass Spectrometry and Electrospray Ionization High-Resolution Tandem Mass Spectrometry, *J. Am. Soc. Mass. Spectrom.* **2020**, *31*, 277-291.
(16) Swanson, D.; Stickle, D.; Evans-Nguyen, T. Analysis of unknown fentanyl analogs using high resolution mass spectrometry with mass defect filtering, *Int. J. Mass spectrom.* **2023**, *485*, 116992.
(17) Wichitnithad, W.; McManus, T. J.; Callery, P. S. Identification of isobaric product ions in electrospray ionization mass spectra of fentanyl using multistage mass spectrometry and deuterium labeling, *Rapid Commun. Mass Spectrom.* **2010**, *24*, 2547-2553.
(18) Denis, E. H.; Bade, J. L.; Renslow, R. S.; Morrison, K. A.; Nims, M. K.; Govind, N.; Ewing, R. G. Proton Affinity Values of Fentanyl and Fentanyl Analogues Pertinent to Ambient Ionization and Detection, *J. Am. Soc. Mass. Spectrom.* **2022**, *33*, 482-490.
(19) Zaknoun, H.; Binette, M.-J.; Tam, M. Analyzing fentanyl and fentanyl analogues by ion mobility spectrometry, *International Journal for Ion Mobility Spectrometry* **2019**, *22*, 1-10.
(20) Butler, K. E.; Baker, E. S. A High-Throughput Ion Mobility Spectrometry–Mass Spectrometry Screening Method for Opioid Profiling, *J. Am. Soc. Mass. Spectrom.* **2022**, *33*, 1904-1913.
(21) Aderorho, R.; Chouinard, C. D. Improved separation of fentanyl isomers using metal cation adducts and high-resolution ion mobility-mass spectrometry, *Drug Testing and Analysis* **2023**, 1-11.
(22) Hollerbach, A. L.; Ibrahim, Y. M.; Lin, V. S.; Schultz, K. J.; Huntley, A. P.; Armentrout, P. B.; Metz, T. O.; Ewing, R. G. Identification of Unique Fragmentation Patterns of Fentanyl Analog Protomers Using Structures for Lossless Ion Manipulations Ion Mobility-Orbitrap Mass Spectrometry, *J. Am. Soc. Mass. Spectrom.* **2024**, *35*, 793-803.
(23) Palmquist, K. B.; Truver, M. T.; Shoff, E. N.; Krotulski, A. J.; Swortwood, M. J. Review of analytical methods for screening and quantification of fentanyl analogs and novel synthetic opioids in biological specimens, *Journal of Forensic Sciences* **2023**, *n/a*.
(24) Strayer, K. E.; Antonides, H. M.; Juhascik, M. P.; Daniulaityte, R.; Sizemore, I. E. LC-MS/MS-Based Method for the Multiplex Detection of 24 Fentanyl Analogues and Metabolites in Whole Blood at Sub ng mL–1 Concentrations, *ACS Omega* **2018**, *3*, 514-523.
(25) Klingberg, J.; Cawley, A.; Shimmon, R.; Fu, S. Collision-Induced Dissociation Studies of Synthetic Opioids for Non-targeted Analysis, *Frontiers in Chemistry* **2019**, *7*.
(26) Schüller, M.; Lucic, I.; Øiestad, Å. M. L.; Pedersen-Bjergaard, S.; Øiestad, E. L. High-throughput quantification of emerging "nitazene" benzimidazole opioid analogs by microextraction and UHPLC–MS-MS, *J. Anal. Toxicol.* **2023**, *47*, 787-796.
(27) Kanamori, T.; Okada, Y.; Segawa, H.; Yamamuro, T.; Kuwayama, K.; Tsujikawa, K.; Iwata, Y. T. Analysis of highly potent synthetic opioid nitazene analogs and their positional isomers, *Drug Testing and Analysis* **2023**, *15*, 449-457.
(28) Hines, K. M.; Ross, D. H.; Davidson, K. L.; Bush, M. F.; Xu, L. Large-Scale Structural Characterization of Drug and Drug-Like Compounds by High-Throughput Ion Mobility-Mass Spectrometry, *Anal. Chem.* **2017**, *89*, 9023-9030.
(29) Kanu, A. B.; Dwivedi, P.; Tam, M.; Matz, L.; Hill Jr., H. H. Ion mobility–mass spectrometry, *J. Mass Spectrom.* **2008**, *43*, 1-22.
(30) Cohen, M. J.; Karasek, F. W. Plasma Chromatography™—A New Dimension for Gas Chromatography and Mass Spectrometry, *J. Chromatogr. Sci.* **1970**, *8*, 330-337.
(31) Boschmans, J.; Jacobs, S.; Williams, J. P.; Palmer, M.; Richardson, K.; Giles, K.; Lapthorn, C.; Herrebout, W. A.; Lemière, F.; Sobott, F. Combining density functional theory (DFT) and

collision cross-section (CCS) calculations to analyze the gas-phase behaviour of small molecules and their protonation site isomers, *Analyst* **2016**, *141*, 4044-4054.
(32) Colby, S. M.; Thomas, D. G.; Nuñez, J. R.; Baxter, D. J.; Glaesemann, K. R.; Brown, J. M.; Pirrung, M. A.; Govind, N.; Teeguarden, J. G.; Metz, T. O.; Renslow, R. S. ISiCLE: A Quantum Chemistry Pipeline for Establishing in Silico Collision Cross Section Libraries, *Anal. Chem.* **2019**, *91*, 4346-4356.
(33) May, J. C.; Knochenmuss, R.; Fjeldsted, J. C.; McLean, J. A. Resolution of Isomeric Mixtures in Ion Mobility Using a Combined Demultiplexing and Peak Deconvolution Technique, *Anal. Chem.* **2020**, *92*, 9482-9492.
(34) Giles, K.; Ujma, J.; Wildgoose, J.; Pringle, S.; Richardson, K.; Langridge, D.; Green, M. A Cyclic Ion Mobility-Mass Spectrometry System, *Anal. Chem.* **2019**, *91*, 8564-8573.
(35) Ridgeway, M. E.; Lubeck, M.; Jordens, J.; Mann, M.; Park, M. A. Trapped ion mobility spectrometry: A short review, *Int. J. Mass spectrom.* **2018**, *425*, 22-35.
(36) Silveira, J. A.; Ridgeway, M. E.; Park, M. A. High Resolution Trapped Ion Mobility Spectrometery of Peptides, *Anal. Chem.* **2014**, *86*, 5624-5627.
(37) Deng, L.; Ibrahim, Y. M.; Hamid, A. M.; Garimella, S. V. B.; Webb, I. K.; Zheng, X.; Prost, S. A.; Sandoval, J. A.; Norheim, R. V.; Anderson, G. A.; Tolmachev, A. V.; Baker, E. S.; Smith, R. D. Ultra-High Resolution Ion Mobility Separations Utilizing Traveling Waves in a 13 m Serpentine Path Length Structures for Lossless Ion Manipulations Module, *Anal. Chem.* **2016**, *88*, 8957-8964.
(38) Deng, L.; Webb, I. K.; Garimella, S. V. B.; Hamid, A. M.; Zheng, X.; Norheim, R. V.; Prost, S. A.; Anderson, G. A.; Sandoval, J. A.; Baker, E. S.; Ibrahim, Y. M.; Smith, R. D. Serpentine Ultralong Path with Extended Routing (SUPER) High Resolution Traveling Wave Ion Mobility-MS using Structures for Lossless Ion Manipulations, *Anal. Chem.* **2017**, *89*, 4628-4634.
(39) Hollerbach, A. L.; Li, A.; Prabhakaran, A.; Nagy, G.; Harrilal, C. P.; Conant, C. R.; Norheim, R. V.; Schimelfenig, C. E.; Anderson, G. A.; Garimella, S. V. B.; Smith, R. D.; Ibrahim, Y. M. Ultra-High-Resolution Ion Mobility Separations Over Extended Path Lengths and Mobility Ranges Achieved using a Multilevel Structures for Lossless Ion Manipulations Module, *Anal. Chem.* **2020**, *92*, 7972-7979.
(40) Wojcik, R.; Nagy, G.; Attah, I. K.; Webb, I. K.; Garimella, S. V. B.; Weitz, K. K.; Hollerbach, A.; Monroe, M. E.; Ligare, M. R.; Nielson, F. F.; Norheim, R. V.; Renslow, R. S.; Metz, T. O.; Ibrahim, Y. M.; Smith, R. D. SLIM Ultrahigh Resolution Ion Mobility Spectrometry Separations of Isotopologues and Isotopomers Reveal Mobility Shifts due to Mass Distribution Changes, *Anal. Chem.* **2019**, *91*, 11952-11962.
(41) Chen, H.; Chen, C.; Huang, W.; Li, M.; Xiao, Y.; Jiang, D.; Li, H. Miniaturized Ion Mobility Spectrometer with a Dual-Compression Tristate Ion Shutter for On-Site Rapid Screening of Fentanyl Drug Mixtures, *Anal. Chem.* **2019**, *91*, 9138-9146.
(42) Demireva, M.; Armentrout, P. B. Relative Energetics of the Gas Phase Protomers of p-Aminobenzoic Acid and the Effect of Protonation Site on Fragmentation, *The Journal of Physical Chemistry A* **2021**, *125*, 2849-2865.
(43) Aderorho, R.; Chouinard, C. D. Determining protonation site in fentanyl protomers using ion mobility-aligned MS/MS fragmentation, *Int. J. Mass spectrom.* **2024**, *496*, 117185.
(44) Ewing, R. G.; Eiceman, G. A.; Harden, C. S.; Stone, J. A. The kinetics of the decompositions of the proton bound dimers of 1,4-dimethylpyridine and dimethyl methylphosphonate from atmospheric pressure ion mobility spectra, *Int. J. Mass spectrom.* **2006**, *255-256*, 76-85.

(45) Fernández-Maestre, R.; Harden, C. S.; Ewing, R. G.; Crawford, C. L.; Hill, H. H. Chemical standards in ion mobility spectrometry, *Analyst* **2010**, *135*, 1433-1442.
(46) Warnke, S.; Seo, J.; Boschmans, J.; Sobott, F.; Scrivens, J. H.; Bleiholder, C.; Bowers, M. T.; Gewinner, S.; Schöllkopf, W.; Pagel, K.; von Helden, G. Protomers of Benzocaine: Solvent and Permittivity Dependence, *Journal of the American Chemical Society* **2015**, *137*, 4236-4242.
(47) Hollerbach, A. L.; Ibrahim, Y. M.; Meras, V.; Norheim, R. V.; Huntley, A. P.; Anderson, G. A.; Metz, T. O.; Ewing, R. G.; Smith, R. D. A Dual-Gated Structures for Lossless Ion Manipulations-Ion Mobility Orbitrap Mass Spectrometry Platform for Combined Ultra-High-Resolution Molecular Analysis, *Anal. Chem.* **2023**, *95*, 9531-9538.
(48) Karasek, F. W.; Hill, H. H.; Kim, S. H. Plasma chromatography of heroin and cocaine with mass-identified mobility spectra, *J. Chromatogr. A* **1976**, *117*, 327-336.
(49) Kelly, R. T.; Page, J. S.; Luo, Q.; Moore, R. J.; Orton, D. J.; Tang, K.; Smith, R. D. Chemically etched open tubular and monolithic emitters for nanoelectrospray ionization mass spectrometry, *Anal. Chem.* **2006**, *78*, 7796-7801.
(50) Chambers, M. C.; Maclean, B.; Burke, R.; Amodei, D.; Ruderman, D. L.; Neumann, S.; Gatto, L.; Fischer, B.; Pratt, B.; Egertson, J.; Hoff, K.; Kessner, D.; Tasman, N.; Shulman, N.; Frewen, B.; Baker, T. A.; Brusniak, M.-Y.; Paulse, C.; Creasy, D.; Flashner, L., et al. A cross-platform toolkit for mass spectrometry and proteomics, *Nat. Biotechnol.* **2012**, *30*, 918-920.
(51) Ewing, R. G.; Atkinson, D. A.; Eiceman, G. A.; Ewing, G. J. A critical review of ion mobility spectrometry for the detection of explosives and explosive related compounds, *Talanta* **2001**, *54*, 515-529.

For Table of Contents Only